Hydrogen storage in calcium alanate: First-principles thermodynamics and crystal structures

Christopher Wolverton
Ford Research and Advanced Engineering, MD 3083/SLR, P.O. Box 2053, Dearborn, Michigan 48121-2053, USA

Vidvuds Ozoliņš
Department of Materials Science and Engineering, University of California, Los Angeles, California 90095-1595, USA
(Received 1 September 2006; published 1 February 2007)

Using first-principles density functional theory (DFT) calculations, we study the thermodynamics and crystal structure of calcium alanate, $Ca(AlH_4)_2$, and its decomposition products $CaAlH_5$, CaH_2, and $CaAl_2$. Using a large database of AB_2C_8 and ABC_5 structure types, we perform nearly 200 DFT calculations in an effort to predict the crystal structures of the $Ca(AlH_4)_2$ and $CaAlH_5$ phases. For the low-energy $T=0$ K phases, we perform DFT frozen-phonon calculations to ascertain the zero-point and vibrational entropy contributions to the thermodynamics of decomposition. We find the following: (i) For $Ca(AlH_4)_2$, we confirm the previously predicted CaB_2F_8-type structure as the stable phase. In addition, we uncover several phases (e.g., β-$ThMo_2O_8$-type, $AgAu_2F_8$-type, and $PbRe_2O_8$-type) very competitive in energy with the ground state structure. (ii) For $CaAlH_5$, we find the stable structure type to be the recently observed α'-$SrAlF_5$-type, with $UTlF_5$-type, $SrFeF_5$-type and $BaGaF_5$-type structures being close in energy to the ground state. (iii) In agreement with recent experiments, our calculations show that the decomposition of $Ca(AlH_4)_2$ is divided into a weakly exothermic step $[Ca(AlH_4)_2 \rightarrow CaAlH_5 + Al + 3/2H_2]$, a weakly endothermic step $[CaAlH_5 \rightarrow CaH_2 + Al + 3/2H_2]$, and a strong endothermic step $[CaH_2 + 2Al \rightarrow CaAl_2 + H_2]$. (iv) Including static $T=0$ K energies, zero-point energies, and the dynamic contributions of H_2 gas, the DFT-calculated ΔH values for the first two decomposition steps (−9 and +26 kJ/mol H_2 at the observed decomposition temperatures $T \sim 127$ and 250 °C, respectively) agree well with the experimental values recently reported (−7 and +32 kJ/mol H_2). Only the second step $[CaAlH_5/CaH_2]$ has thermodynamics near the targeted range that might make a suitable on-board hydrogen storage reaction for hydrogen-fueled vehicles. (v) Comparing the enthalpies for final stage of decomposition $[CaH_2 + 2Al \rightarrow CaAl_2 + H_2, \Delta H = 72$ kJ/mol $H_2]$ with the pure decomposition of CaH_2 $[CaH_2 \rightarrow Ca + H_2, \Delta H = 171$ kJ/mol $H_2]$ shows that the addition of Al provides a huge destabilizing effect on CaH_2, due to the formation of the strongly bound $CaAl_2$ phase.

DOI: 10.1103/PhysRevB.75.064101 PACS number(s): 61.66.−f

I. INTRODUCTION

Hydrogen internal-combustion engine and hydrogen fuel cell vehicles are both reliant on an efficient means of storing hydrogen as a fuel on board the vehicle. The targeted hydrogen storage density for on-board applications far outpaces the currently available technologies, both by volume and by weight.[1] Thus, there is currently a large worldwide research effort directed towards finding a suitable means of storing hydrogen for hydrogen-fueled vehicles.[2]

Following the discovery of reversible H_2 storage in Ti-doped sodium alanate by Bogdanovic and Schwickardi[3] in 1997, there has been a strong interest in $NaAlH_4$ (7.4 total wt % H_2) and other higher-density alanates. $NaAlH_4$ decomposes to liberate three-fourths of its total hydrogen in a reversible two-step process:

$$NaAlH_4 \rightarrow \frac{1}{3}Na_3AlH_6 + \frac{2}{3}Al + H_2$$

$$\rightarrow NaH + Al + \frac{3}{2}H_2 \quad (5.6 \text{ wt } \%\ H_2). \qquad (1)$$

By replacing Na^+ with a lighter Li^+ cation, one can increase the theoretical density of hydrogen in the compound. Unfortunately, hydrogen storage in this higher-density alanate $LiAlH_4$ (10.5 total wt % H_2) has so far met with limited success: Thermal decomposition of this compound occurs in a set of two-step reactions analogous to Eq. (1)—i.e., with the alanate decomposing first to a hexahydride Li_3AlH_6 and subsequently to the monohydride LiH.[4] However, attempts to rehydride a mixture of LiH and Al back into $LiAlH_4$ with moderate pressure and temperature have generally proved unsuccessful, and thermodynamic considerations indicate that $LiAlH_4$ is simply too unstable to easily rehydride.

Another possibility for improved densities is to replace Na^+ with a divalent cation—e.g., Mg^{2+} or Ca^{2+}. These divalent alanates contain higher total hydrogen content by weight $[Mg(AlH_4)_2$, 13.5 total wt % H_2, and $Ca(AlH_4)_2$, 7.8 total wt % $H_2]$ than sodium alanate, despite the fact that both Mg and Ca are heavier than Na. This increased density is, of course, due to the fact that twice as many $(AlH_4)^-$ complex anions are present in the divalent alanates. However, studies of Mg alanate[5] have shown that, similar to Li alanate, the thermodynamics of desorption are poor, and though a significant amount of H_2 can be desorbed from $Mg(AlH_4)_2$, rehydriding this compound remains problematic.

Calcium alanate, $Ca(AlH_4)_2$, has been far less studied. The compound was first synthesized in the 1950s,[6] but only in the past few years have its structural and storage properties been investigated.[7] Very recently, Mamatha *et al.*[8] have synthesized $Ca(AlH_4)_2$ and studied its decomposition using x-ray diffraction (XRD), NMR, and IR spectroscopies and

 ©2007 The American Physical Society

differential scanning calorimetry (DSC). These authors proposed the following three-step decomposition reactions:

$$\mathrm{Ca(AlH_4)_2} \rightarrow \mathrm{CaAlH_5} + \mathrm{Al} + \frac{3}{2}\mathrm{H_2} \rightarrow \mathrm{CaH_2} + 2\mathrm{Al} + 3\mathrm{H_2}$$
$$\rightarrow \mathrm{CaAl_2} + 4\mathrm{H_2}. \quad (2)$$

From their DSC results, they extracted the enthalpies of the first and second steps as being slightly exothermic (−7 kJ/mol H_2) and endothermic (+32 kJ/mol H_2), respectively.

In this paper, we wish to study the structure and thermodynamics of the decomposition reactions for calcium alanate [Eq. (2)] using a first-principles density functional theory (DFT) approach. The crystal structure of $Ca(AlH_4)_2$ is experimentally unknown, and that of $CaAlH_5$ has only recently been determined. Using a large database of candidate AB_2C_8 and ABC_5 crystal structure types, we perform nearly 200 DFT calculations in an effort to predict the low-energy crystal structures. We note that an analogous theoretical study has been performed to elucidate the structure of $Ca(AlH_4)_2$.[9] Using a much larger set of potential input structures, we confirm the low-energy structure found in this previous study and also identify several structures competitive in energy. We also confirm the recently observed[10] structure of $CaAlH_5$. For the low-energy $T=0$ K phases, we perform DFT frozen-phonon calculations to ascertain the zero-point and vibrational entropy contributions to the thermodynamics of decomposition. We generally find agreement with recent experiments, and our calculations show that the three-step decomposition of $Ca(AlH_4)_2$ is divided into a weakly exothermic first step, a mildly endothermic second step, and a strongly endothermic third step (−9, +23, and +72 kJ/mol H_2 at $T=300$ K).

II. METHODOLOGY

Our electronic-structure total energy calculations are based on DFT,[11] as implemented in the highly efficient VASP code.[12] Core-electron interactions are described by either ultrasoft pseudopotentials[13] or projector augmented-wave (PAW) potentials.[14] For exchange correlation, we use the generalized gradient approximation (GGA) of Perdew and Wang,[15] as we have previously[16] shown the GGA to be superior to the local density approximation for calculating the thermodynamic properties of hydrogen storage materials. We optimize all atomic positions, cell shape, and cell volume.

Structural properties were computed using VASP PAW-GGA potentials Ca_sv, Al, and H_h, with *s* and *p* semicore states treated as valence for Ca and a hard H potential. We use the PREC=high setting (plane-wave basis cutoff energy of 875 eV) in all calculations. $4\times4\times4$ or better Monkhorst-Pack *k*-point meshes were used for all structures. All structural degrees of freedom were relaxed within the constraints of the space group of the prototype structure until the energy differences between successive conjugate gradient iterations were below 1 meV. Vibrational spectra were obtained using the frozen-phonon technique. For the phonon calculations, we used ultrasoft (US) GGA pseudopotentials Ca_pv, Al_h, H_200 eV, with *p* semicore states treated as valence for Ca and a softer H potential. We use a plane-wave basis cutoff of 500 eV and an augmentation charge cutoff of 1000 eV. We checked that the US-GGA enthalpies for the Ca alanate decomposition reactions were the same as the PAW-GGA enthalpies, to within better than 1 kJ/mol H_2. The low-energy structures used in the frozen-phonon calculations were relaxed until the forces were below 10 meV/Å and stresses were below 1 kbar. Subsequently, each symmetry-inequivalent atom was displaced along all symmetry-inequivalent directions and forces on all atoms were calculated to obtain a row of the dynamical matrix. We used five displacements separated by 0.03 Å, lying symmetrically around the equilibrium position. The forces were fit to third-order splines, and the linear term was used to construct the dynamical matrix. We found that increasing the augmentation cutoff to 1000 eV helped enforce translational invariance and obtain an accurate representation of the low-frequency phonon spectrum.

The following supercell sizes and shapes (in terms of the primitive cell vectors) were used to calculate phonons:

Compound	Prototype structure	Supercell	Number of atoms
$Ca(AlH_4)_2$	CaB_2F_8	$1\times1\times1$	88
	β-$ThMo_2O_8$	$1\times1\times1$	99
	$AgAu_2F_8$	$3\times1\times2$	132
	$PbRe_2O_8$	$1\times1\times3$	99
$CaAlH_5$	α'-$SrAlF_5$	$1\times1\times1$	56
	$UTlF_5$	$1\times1\times1$	56
	$BaGaF_5$	$1\times2\times2$	112
	$SrFeF_5$	$1\times1\times1$	56
CaH_2	Co_2Si	$2\times4\times2$	192
$CaAl_2$	Cu_2Mg	$2\times2\times2$	48
Al	Cu	$4\times4\times4$	64
Ca	Cu	$6\times6\times6$	216

The vibrational energy calculation for the H_2 dimer was performed in a rectangular box of dimensions $16\times14\times14$ Å^3. The dimer was oriented along the longer edge.

III. RESULTS: DFT CALCULATIONS

A. Crystal structure databases for AB_2C_8 and ABC_5 stoichiometries

First-principles DFT calculations of total crystal binding energies are well suited to predict hydriding enthalpies of H_2 storage materials.[16] In order to predict the energetics of the decomposition of H_2 storage compounds such as $Ca(AlH_4)_2$ and $CaAlH_5$, one first has to know the energy and hence the crystal structure of these phases. Since one of these structures is not known experimentally, and the other has only recently been reported,[10] we search for low-energy crystal structures by using structures of chemically similar compounds from the International Crystal Structures Database (ICSD).

AB_2C_8 stoichiometry. From the ICSD, we find a set of

candidate crystal structures for compounds of stoichiometry AB_2C_8 where C=H/D, F, Cl, Br, I, and O. In addition to the ICSD structures, we also include the recently proposed structures of $Mg(AlH_4)_2$ (Ref. 17) and $Ca(AlH_4)_2$ (Ref. 9) (see text below) in our set of candidates. In total, we construct a set of 93 *candidate* AB_2C_8 *structures*. Note that when more than one entry in the ICSD database exists for a given structure, we often take more than one (see below for a discussion of symmetrically distinct structures) and simply label them as "_2," "_3," etc. The structures that we use for this AB_2C_8 stoichiometry include $AgAu_2F_8$, $Ba_2B_4F_{16}$, $BaAl_2Cl_8$, $BaAu_2F_8$, $BaFe_2Br_8$, $BaMn_2O_8$_1, $BaMn_2O_8$_2, $BaTm_2F_8$, BeB_2H_8, $CaAl_2Cl_8$, $CaAl_2H_8$, CaB_2F_8, CaB_2H_8, $CdAl_2Cl_8$, $CdAl_2Cl_8$_2, $CdAu_2F_8$, $CeSe_2O_8$, $CoAl_2Cl_8$_1, $CoAl_2Cl_8$_2, $CoAl_2Cl_8$_3, $CoAl_2Cl_8$_4, $CoCl_2O_8$, $CoRe_2O_8$, $CuAl_2Cl_8$_1, $CuAl_2Cl_8$_2, $CuAl_2Cl_8$_3, $CuAl_2Cl_8$_4, $CuAl_2Cl_8$_5, $CuGa_2Cl_8$, $CuGa_2Cl_8$_1, $EuAl_2Cl_8$, $HfMo_2O_8$_1, $HfMo_2O_8$_2, $HgAu_2F_8$, $MgAl_2Cl_8$, $MgAl_2H_8$, $MgAu_2F_8$, MnB_2F_8, $MnRe_2O_8$, MoV_2O_8_2, MoV_2O_8_3, $NiAu_2F_8$_1, $NiAu_2F_8$_2, $NiCl_2O_8$, $NiRe_2O_8$, $PbRe_2O_8$, $PdAl_2Cl_8$, $PdAl_2Cl_8$_2, $PdAu_2F_8$, $PdGa_2Br_8$, $PdGa_2I_8$, PtS_2Cl_8, ReK_2F_8, $SmAl_2Cl_8$, $SrAl_2Cl_8$_1, $SrAl_2Cl_8$_2, $SrAl_2Cl_8$_3, $SrAl_2Cl_8$_4, $SrAl_2Cl_8$_5, $SrAl_2Cl_8$_6, $TbCd_2F_8$, $ThMo_2O_8$_1, $ThMo_2O_8$_2, $ThMo_2O_8$_3, $ThMo_2O_8$_4, $TiAl_2Br_8$_1, $TiAl_2Br_8$_2, $TiAl_2Cl_8$_1, $TiAl_2Cl_8$_2, $TiAl_2Cl_8$_3, $TiAl_3Cl_8$_4, UI_2O_8, UMo_2O_8_1, UMo_2O_8_2, UMo_2O_8_3, UTa_2O_8, UV_2O_8, UW_2O_8, WK_2O_8, WP_2O_8_1, WP_2O_8_2, $YbAl_2Cl_8$, $ZnAu_2F_8$, $ZnRe_2O_8$, $ZrBa_2F_8$, $ZrMo_2O_8$_1, $ZrMo_2O_8$_2, $ZrMo_2O_8$_3, $ZrMo_2O_8$_4, $ZrPb_2F_8$, ZrS_2O_8, ZrW_2O_8_1, and ZrW_2O_8_2.

ABC_5 *stoichiometry*. From the ICSD, we find a set of candidate crystal structures for compounds of stoichiometry ABC_5 where C=F, H/D, Cl, S, Br, Te, and O. This set contains *84 candidate* ABC_5 *structures*. The structures that we use for this ABC_5 stoichiometry include $AgAgF_5$_1, $AgAgF_5$_2, $AgBF_5$, $AgPO_5$, $AuCuF_5$, $AuKS_5$, $AuSCl_5$, $BaAlD_5$, $BaAlF_5$, $BaCrF_5$, $BaFeF_5$, $BaGaF_5$, $BaGdCl_5$, $BaMnF_5$, $BaSbF_5$, $CaAlF_5$, $CaCrF_5$, $CaFeF_5$, $CaMnF_5$, $CaTiF_5$, $CdMnF_5$, Cr_2F_5, $CrMnF_5$, $CsTbF_5$, $CsTeF_5$, $CuAuF_5$, CUO_5, $FeAlF_5$, $INpO_5$, $KAuS_5$, $KTbF_5$, $KTeF_5$, $KZrF_5$, La_2Br_5, $LiUF_5$, $MnAlF_5$, $MnCrF_5$, $MoUO_5$, $NaTeF_5$, $NbPO_5$, $NbPO_5$_2, $NiTaTe_5$, $NpIO_5$, $PAsO_5$, $PNbO_5$, $PNbO_5$_2, $PTaO_5$, PVO_5, PVO_5_2, PWO_5, $RbSF_5$, $RbTeF_5$, $SAuCl_5$, $SeUO_5$, α'-$SrAlF_5$, $SrAlF_5$, $SRbF_5$, $SrFeF_5$, $SRhCl_5$, $SrSbF_5$, $STiO_5$, SVO_5, $TaNiTe_5$, $TaPO_5$, $TbCsF_5$, $TbKF_5$, $TeCsF_5$, $TeKF_5$, $TeNaF_5$, $TeRbF_5$, $TeTlF_5$, $TeUO_5$, $TiSO_5$, UCO_5, $ULiF_5$, $UMoO_5$, $USeO_5$, $UTeO_5$, $UTlF_5$, VPO_5, VPO_5_2, VSO_5, WPO_5, and $ZrKF_5$.

We note several things about our set of candidate structures. Some chemical compositions appear more than once in the ICSD database. In some cases, these are actually different structure types that exist under different conditions (e.g., high- versus low-temperature or high- versus low-pressure phases). However, in other cases, they are merely multiple reports of the same structure, with different lattice parameters or other structural parameters. We retain many of these isostoichiometric structures, with the knowledge that we may simply have some redundant structure types in our database. Below, we describe our method to sort out the number of truly distinct structures. In all cases, we relaxed structures consistent with the initial symmetry of the starting structure. Another strategy to more fully explore the space of possible structure topologies would be to relax each structure without considering symmetry constraints (i.e., relaxing the structure with a $P1$ symmetry). Vajeeston *et al.*[18] and Løvvik and Swang[18] have described the differences between these two types of relaxation approaches for predicting new structure types. These authors assert that a smaller set of input structures may be used when relaxing with $P1$ symmetry. However, we also note that in his search for the $Ca(AlH_4)_2$ structure type, Lovvik[9] used a very small set of input structures (seven) and used both relaxation schemes. In that case, relaxing with $P1$ symmetry did not produce any substantially new results or any significant energy lowering in any of the structures. Hence, our 93 AB_2C_8 and 84 ABC_5 structural candidates should provide a large and thorough set of topologies capable of providing an excellent prediction of the ground state properties of the $Ca(AlH_4)_2$ and $CaAlH_5$ phases.

In order to distinguish whether the various DFT calculations relax to truly distinct structure types, we monitor not only the total energy for each relaxed configuration, but also symmetry information via the Pearson symbol (a measure of the symmetry, lattice type, and number of atoms in the unit cell). Note that in the Pearson symbols in this paper, we list the number of atoms in the *primitive* unit cell, rather than the *conventional* unit cell. We consider structures to be equivalent when two different relaxed calculations give configurations which possess identical Pearson symbols and degenerate energies (within 1 kJ/mol formula unit).

We next describe the results of the DFT energetics for $Ca(AlH_4)_2$ and $CaAlH_5$ computed using the sets of candidate structure types described above.

B. $Ca(AlH_4)_2$: Crystal structures

Using DFT calculations, we have determined the total energies, lattice parameters, and atomic positions of $Ca(AlH_4)_2$ in each one of the 93 AB_2C_8 candidate crystal structures. After relaxation, we find 49 distinct structures and energies (distinct Pearson symbols or energies which differ by more than 1 kJ/mol formula unit). These distinct structures and energies are given in Table I. The crystal structure with the lowest energy was used as an approximation of the ground-state energy and crystal structure of the $Ca(AlH_4)_2$ compound. Our lowest-energy structure is the CaB_2F_8 type. This structure is primitive orthorhombic, with space group *Pbca* and 88 atoms per unit cell. We note that several of the candidates ($CaAl_2H_8$, $ThMo_2O_8$_3, $ThMo_2O_8$_1, $CeSe_2O_8$, UW_2O_8, and CaB_2F_8) in our database are isostructural with CaB_2F_8 and therefore relax to the same ground-state structure and energy as the CaB_2F_8 calculation. One of these isostructural candidates is the α-$ThMo_2O_8$-type structure. In addition to the ground-state structure, we find three phases that are very competitive in energy with the ground state (they differ in energy by less than 10 kJ/mol formula unit): β-$ThMo_2O_8$ type, $AgAu_2F_8$ type, and $PbRe_2O_8$ type. Given that the lowest-energy structure found is α-$ThMo_2O_8$ type, it is quite interesting that the β-$ThMo_2O_8$-type phase is also competitive in energy. In the Th-Mo-O system, the β-

TABLE I. Energetics and Pearson symbols for $Ca(AlH_4)_2$ calculated in each of the structures in our database of 93 AB_2C_8 compounds. Energies are given in kJ/formula unit, relative to the lowest-energy CaB_2F_8-type structure. Structures with identical Pearson symbols and relaxed energies with 1 kJ/mol of formula unit were considered equivalent. Only the results for 49 distinct structures and energies are shown here. Note that in the Pearson symbols, we list the number of atoms in the primitive unit cell, rather than the conventional unit cell. We also note that $ThMo_2O_8$_4 in this table corresponds to the β-$ThMo_2O_8$ structure, discussed in the text.

Structure	Energy	Pearson symbol
CaB_2F_8	0.00	oP88
$ThMo_2O_8$_4	5.13	hP99
$AgAu_2F_8$	8.56	mP22
$PbRe_2O_8$	9.12	hP33
$NiAu_2F_8$_2	11.19	mP22
MnB_2F_8	15.97	oP44
$CuAl_2Cl_8$_4	18.32	mP22
$CuAl_2Cl_8$_2	18.44	aP22
$Ba_2B_4F_{16}$	22.30	mP88
$TiAl_2Cl_8$_2	24.22	mC22
$NiCl_2O_8$	24.52	hR11
$TbCd_2F_8$	24.85	tI11
ZrW_2O_8_1	24.99	cP44
$SmAl_2Cl_8$	25.26	mP22
CaB_2H_8	25.81	cF11
$BaAl_2Cl_8$	26.26	mP22
$CoCl_2O_8$	26.83	hR11
$PdAu_2F_8$	28.57	mP22
$BaMn_2O_8$_1	28.77	oF22
PtS_2Cl_8	30.94	mP22
ZrW_2O_8_2	35.49	oP132
$ZrMo_2O_8$_1	37.74	hP66
$TiAl_2Br_8$_1	38.17	oP22
$ZrMo_2O_8$_4	38.59	mC11
$MgAl_2H_8$	38.75	aP11
$ZnRe_2O_8$	38.93	hP11
UI_2O_8	39.40	mP22
$BaFe_2Br_8$	40.17	oP88
WK_2O_8	42.98	hR66
BeB_2H_8	43.37	tI88
$BaAu_2F_8$	45.23	tI22
$ZrMo_2O_8$_3	45.44	oP22
$HfMo_2O_8$_2	45.57	mC22
$ThMo_2O_8$_2	49.54	hP99
$CdAl_2Cl_8$_2	50.26	mP22
$PdGa_2Br_8$	50.95	mC11
$CaAl_2Cl_8$	60.13	tI44
$SrAl_2Cl_8$_2	60.43	oP88
$SrAl_2Cl_8$_1	62.51	tI44
UMo_2O_8_3	87.20	oP44
UV_2O_8	93.62	oP44
$ZrBa_2F_8$	101.28	oP44
WP_2O_8_1	106.78	mC22
MoV_2O_8_2	115.10	oC11
$HfMo_2O_8$_1	126.02	hP66
MoV_2O_8_3	131.29	mC11
$CdAu_2F_8$	193.01	tP22
ReK_2F_8	198.94	oP44
UTa_2O_8	333.32	hP11

$ThMo_2O_8$ structure is a high-temperature phase, whereas the α-$ThMo_2O_8$ is stable at low temperatures.[19] This analogy with $Ca(AlH_4)_2$ is interesting, in that it could suggest a possible temperature-induced structural phase transformation in this system. We also note that the structures found are not necessarily from "intuitive" or chemically similar systems. In other words, it seems unlikely that one would have guessed *a priori* that the Th-Mo-O system was a good place to find likely structural candidates for the Ca-Al-H system.

We note that Løvvik[9] performed a similar DFT study to search for the structure of $Ca(AlH_4)_2$, though his set of seven input structures was somewhat limited. Our lowest-energy $Ca(AlH_4)_2$ structure (CaB_2F_8 type) is the same as the one Løvvik found. Thus, our calculations confirm this previous result, but our much larger set of input structures provides more confidence in the validity of this prediction. Table II contains full structural details for our predicted low-energy $Ca(AlH_4)_2$ structures.

The low-energy $Ca(AlH_4)_2$ structures contain a variety of Al-H coordinations and bond lengths. Two of the low-energy structures contain Al fourfold coordinated by H in $(AlH_4)^-$ complexes that one might expect. Specifically, the CaB_2F_8-type structure contains only slightly distorted AlH_4 tetrahedra with Al-H bond lengths between 1.62 and 1.63 Å. The β-$ThMo_2O_8$-type structure also contains AlH_4 tetrahedra that are only slightly distorted with Al-H bonds lengths between 1.61 and 1.63 Å. However, somewhat surprisingly, the $AgAu_2F_8$-type structure contains sixfold-coordinated AlH_6 units that are highly distorted octahedra with Al-H distances ranging from 1.67 to 1.82 Å; and the most unusual structure $PbRe_2O_8$-type contains fivefold-coordinated AlH_5 units with three short Al-H bonds (1.61–1.67 Å) and two long Al-H bonds (1.80–1.81 Å). These structures are depicted in Fig. 1.

C. $CaAlH_5$: Crystal structures

Using a similar procedure to that outlined above for $Ca(AlH_4)_2$, we have used first-principles DFT calculations to scan through and determine the energetics of $CaAlH_5$ in each of the 84 candidate ABC_5 structures; from this search, we

TABLE II. Structural parameters for predicted low-energy $Ca(AlH_4)_2$ and $CaAlH_5$ compounds.

Stoichiometry	Prototype	Space group	Lattice parameters (Å)	Atomic positions			
					x	y	z
$Ca(AlH_4)_2$	CaB_2F_8	$Pbca$	$a=13.4084$	Ca	0.6048	0.5338	0.7214
			$b=9.5622$	Al	0.4387	0.7719	0.4988
			$c=8.9470$	Al	0.6545	0.8908	0.8115
				H	0.4810	0.6567	0.6166
				H	0.6315	0.3845	0.9146
				H	0.6282	0.3152	0.6204
				H	0.5314	0.6492	0.9177
				H	0.6579	0.9125	0.9908
				H	0.5410	0.9155	0.7497
				H	0.6873	0.7336	0.7661
				H	0.7275	0.0031	0.7309
$Ca(AlH_4)_2$	β-$ThMo_2O_8$	$P\bar{3}$	$a=15.8098$	Ca	0.3343	0.3340	0.7504
			$c=5.9036$	Ca	0.6666	0.3333	0.5096
				Ca	0.0000	0.0000	0.0000
				Al	0.2667	0.4324	0.2327
				Al	0.5994	0.0999	0.2527
				Al	0.2368	0.1703	0.2639
				H	0.0186	0.2298	0.4889
				H	0.4399	0.1126	0.9959
				H	0.7484	0.0024	0.0723
				H	0.6451	0.0974	0.0092
				H	0.4863	0.0156	0.2767
				H	0.9235	0.0521	0.2162
				H	0.3206	0.4175	0.4502
				H	0.6675	0.0945	0.4538
				H	0.2778	0.5404	0.2627
				H	0.1526	0.3499	0.2215
				H	0.3179	0.1369	0.2489
				H	0.6104	0.2079	0.2780
$Ca(AlH_4)_2$	$AgAu_2F_8$	$P2_1/c$	$a=6.2586$	Ca	0.5000	0.5000	0.5000
			$b=11.8096$	Al	−0.1789	−0.1845	−0.0552
			$c=4.3673$	H	0.0193	−0.0789	0.3383
			$\beta=137.9329$	H	−0.4487	−0.0928	−0.4784
				H	0.0410	−0.2950	0.3519
				H	−0.4086	−0.3013	−0.4598
$Ca(AlH_4)_2$	$PbRe_2O_8$	$P\bar{6}2m$	$a=10.3169$	Ca	0.0000	0.0000	0.0000
			$c=3.6004$	Ca	0.3333	0.6666	0.5000
				Al	0.3890	0.0000	0.0000
				Al	0.7186	0.0000	0.5000
				H	0.5467	0.1667	0.0000
				H	0.7292	0.1610	0.5000
				H	0.2325	0.0000	0.0000
				H	0.7287	0.0000	0.0000
				H	0.8762	0.0000	0.5000
				H	0.4095	0.0000	0.5000
$CaAlH_5$	α'-$SrAlF_5$	$P2_1/n$	$a=8.334$	Ca	0.2624	0.2307	0.0436
			$b=6.927$	Ca	0.8114	0.2685	0.1509

TABLE II. (*Continued.*)

Stoichiometry	Prototype	Space group	Lattice parameters (Å)	Atomic positions			
					x	*y*	*z*
			c=9.709	Al	0.5062	0.3054	0.3102
			β=93.88	Al	0.1293	0.2185	0.3433
				H	0.3244	0.1913	0.2762
				H	0.5304	0.2857	0.1384
				H	0.0873	0.3541	0.1974
				H	0.1857	0.4015	0.4543
				H	0.9309	0.2137	0.3703
				H	0.5117	0.6956	0.5168
				H	0.6435	0.1112	0.3378
				H	0.1979	0.0560	0.4638
				H	0.0960	0.0269	0.2137
				H	0.3122	0.5656	0.6643
$CaAlH_5$	$UTlF_5$	*Pbca*	a=6.4213	Ca	1.4847	0.8401	0.1101
			b=10.4618	Al	0.6973	0.6072	0.2507
			c=8.8399	H	0.8505	0.2599	0.3252
				H	0.7223	0.4536	0.1899
				H	0.7387	0.3126	0.5873
				H	1.0559	0.3802	0.6693
				H	1.1047	0.5467	0.0840
$CaAlH_5$	$SrFeF_5$	$P2_1/c$	a=6.2445	Ca	0.6876	0.1623	0.0885
			b=6.6184	Ca	0.0019	0.6490	0.1400
			c=13.2954	Al	0.5100	0.6211	0.1596
			β=94.0397	Al	0.8153	0.6789	0.3746
				H	0.6939	0.4976	0.0934
				H	0.3249	0.6844	0.0646
				H	0.3204	0.6704	0.2407
				H	0.6898	0.5526	0.2693
				H	0.6654	0.8305	0.1533
				H	0.0005	0.4891	0.3885
				H	0.9812	0.8059	0.2943
				H	0.6169	0.8659	0.3528
				H	0.6527	0.5734	0.4578
				H	0.9696	0.8171	0.4655
$CaAlH_5$	$BaGaF_5$	$P2_12_12_1$	a=12.1647	Ca	0.5889	0.1113	0.5315
			b=4.9675	Al	0.6636	0.6291	0.9366
			c=4.3809	H	0.7619	0.1247	1.2703
				H	0.9241	0.1454	0.6029
				H	0.5879	0.3658	1.0733
				H	0.5698	0.6306	0.6363
				H	0.7384	0.3766	0.7289

have used the lowest-energy structure as an approximation of the ground-state energy and crystal structure of the $CaAlH_5$ compound. One interesting ambiguity arises in the case of ABC_5 prototype structures which does not arise in AB_2C_8 prototypes: Two of the sites, the A and B sites, have equal stoichiometries in ABC_5. Hence, there is some ambiguity whether to place Ca on A and Al on B or vice versa. Many structural candidates have prototypes with one 2^+ and one 3^+ cation (e.g., $SrAlF_5$). In those cases, we simply place Ca on the 2^+ site and Al on the 3^+ site. However, other structures have prototypes where there is not a clear division between the $2^+/3^+$ sites (e.g., $CuAuF_5$). In those cases, we simply tried both possibilities: Ca/Al on A/B sites and also Al/Ca on A/B sites.

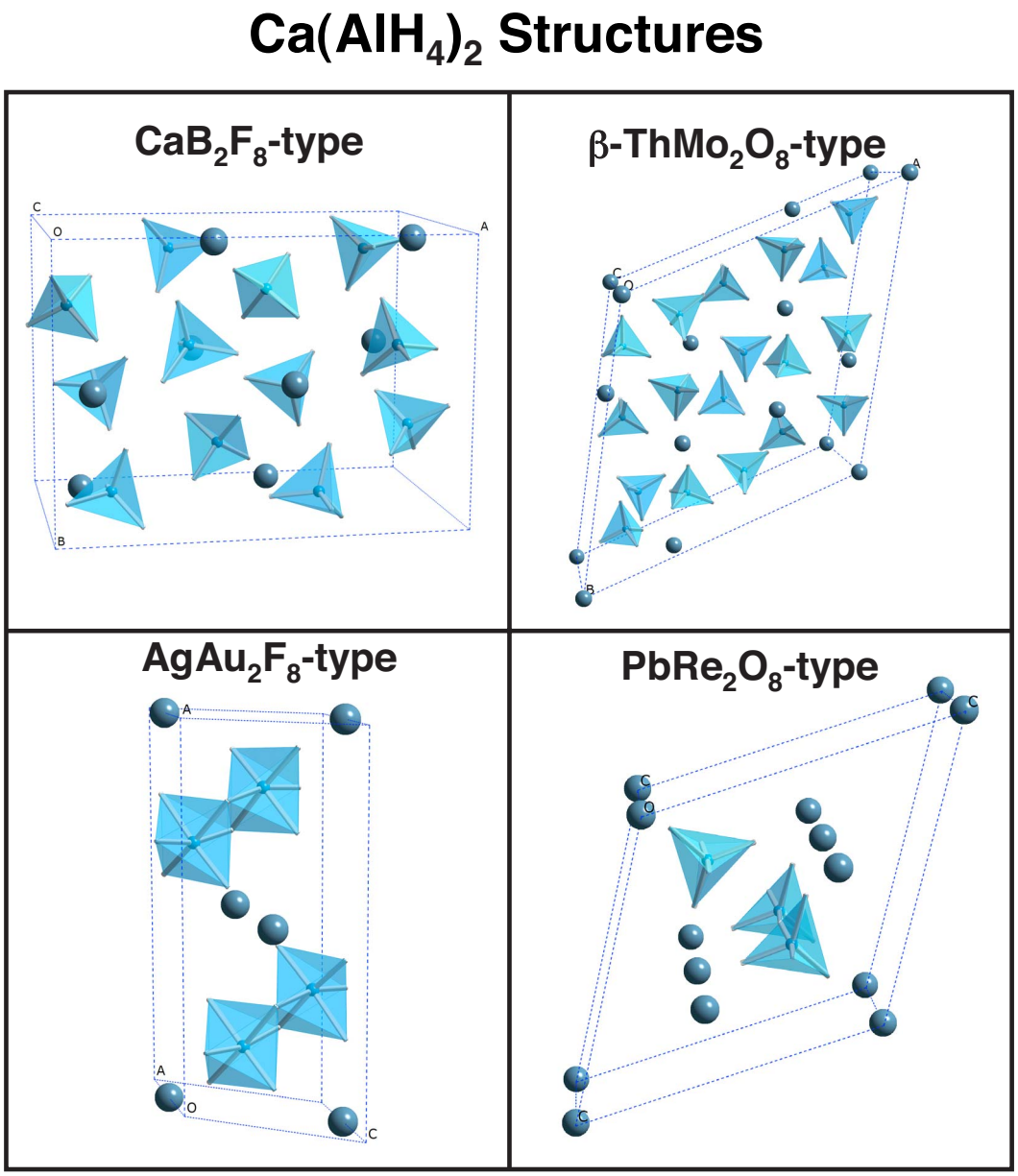

FIG. 1. (Color online) DFT-predicted low-energy structures found for the $Ca(AlH_4)_2$ stoichiometry. Large spheres are Ca atoms, and Al are centered in polyhedra. For visual clarity, H atoms are not shown, but are at vertices of polyhedra.

After relaxation, the 84 $CaAlH_5$ calculations converge to 60 distinct structures and energies. The energetics and Pearson symbols for these 60 distinct structures are given in Table III. We find that the α'-$SrAlF_5$-type structure gives the lowest energy, but there are also three very closely competing structures: $UTlF_5$-type, $SrFeF_5$-type, and $BaGaF_5$-type. These four structures are all extremely close in energy, within 6 kJ/mol formula unit of one another. Again, we note that one of the prototype systems (U–Tl–F) is not necessarily a very intuitive place to look for structural candidates for Ca-Al-H. All four structures possess AlH_6 octahedra which share vertices, but they are joined in topologically different ways (see Fig. 2). In the α'-$SrAlF_5$-type structure, the octahedra have Al-H bond lengths of 1.69–1.84 Å, in the $UTlF_5$-type structure the bond lengths are 1.70–1.78 Å, in the $SrFeF_5$-type structure the bond lengths are 1.69–1.87 Å, and in the $BaGaF_5$-type structure they are 1.69–1.80 Å. Table II contains full structural details for our predicted low-energy $CaAlH_5$ structures.

A recent DFT study[20] of the analogous compounds $MgAlH_5$ and $BaAlH_5$ used a database of 50 structural types similar to our own. The $BaAlH_5$ structure is known experimentally, and these authors predicted that the $MgAlH_5$ compound forms in the $CaFeF_5$-type structure. Though not described in detail here, we have performed an analogous study to the one described above for the $MgAlH_5$ phase and, interestingly, find a different structural candidate as the lowest-energy structure to the one that Klaveness *et al.* proposed.[20] We are currently investigating this discrepancy and examining the effect of exchange correlation on structural predictions of this type.

TABLE III. Energetics and Pearson symbols for $CaAlH_5$ calculated in each of the structures in our database of 84 ABC_5 compounds. Energies are given in kJ/formula unit, relative to the lowest-energy α'-$SrAlF_5$-type structure. Structures with identical Pearson symbols and relaxed energies with 1 kJ/mol formula unit were considered equivalent. Only the results for 60 distinct structures and energies are shown here. Note that in the Pearson symbols, we list the number of atoms in the primitive unit cell, rather than the conventional unit cell.

Structure	Energy (kJ/formula unit)	Pearson symbol
α'-$SrAlF_5$	0	mP56
$UTlF_5$	3.04	mP56
$SrFeF_5$	5.23	mP56
$BaGaF_5$	5.95	oP28
$SrAlF_5$	14.53	tI56
$PTaO_5$	19.04	mP56
$BaAlD_5$	21.30	oP28
$CaFeF_5$	23.15	mP28
$AgAgF_5$_1	25.60	aP28
$TbKF_5$	25.93	aP42
$CuAuF_5$	26.70	aP7
$INpO_5$	28.40	oP28
$SeUO_5$	31.93	mP14
$LiUF_5$	32.64	tI56
$MnCrF_5$	36.50	mC14
$CdMnF_5$	36.51	mP28
SVO_5	36.66	oP28
$USeO_5$	37.11	mP14
$MnAlF_5$	38.18	oC14
$KZrF_5$	38.43	aP42
$FeAlF_5$	44.42	oI7
PWO_5	46.73	oP28
$TeUO_5$	48.99	oP28
$STiO_5$	50.19	mC28
$NaTeF_5$	50.65	oP28
$AgAgF_5$_2	50.90	aP28
$ZrKF_5$	51.83	aP42
$TeNaF_5$	54.18	oP28
$BaGdCl_5$	55.00	mC14
NpIO5	56.84	oP28
$CrMnF_5$	57.67	mC14
PVO_5	57.98	tP14
WPO_5	59.29	oP28
$AuSCl_5$	60.84	mP28
$RbTeF_5$	63.51	oP56
$ULiF_5$	66.50	tI56
$SRhCl_5$	67.90	mC84
$UTeO_5$	71.16	oP28
$AgBF_5$	72.14	tP14
CUO_5	72.57	oI7
VPO_5	72.69	tP14
$AgPO_5$	74.23	oP28
$NbPO_5$_2	76.40	oP28
$TaPO_5$	76.78	mP56
$TiSO_5$	77.46	mC28
VSO_5	78.09	oP28
$CsTbF_5$	79.18	oC28
$TeRbF_5$	79.99	oP56
$TeTlF_5$	82.66	oP28
$TeKF_5$	85.00	oP28
$TaNiTe_5$	92.51	oC14
$UMoO_5$	94.77	oP28
$TeCsF_5$	97.25	oP28
$MoUO_5$	138.48	oP28
$LaLaBr_5$	155.92	mP14
$KAuS_5$	193.76	oI28
$CrCrF_5$	195.57	mC14
$NiTaTe_5$	242.60	oC14
$AuKS_5$	297.84	oI28
$TbCsF_5$	356.76	oC28

The structure proposed in this work for $Ca(AlH_4)_2$ is a DFT prediction, and there are no experimentally measured structures with which to compare. In contrast, the structures of CaH_2 and $CaAl_2$ are experimentally well established and $CaAlH_5$ has recently been reported,[10] and we can compare the structural details of our DFT calculations with experimental data for these compounds. The comparisons are given in Table IV, which shows that the DFT structural parameters are in excellent agreement with experiment.

D. Energetics and thermodynamics of $Ca(AlH_4)_2$ decomposition

We next evaluate the energetics of decomposition in the calcium alanate system. We begin with the static, $T=0$ K energetics and subsequently discuss the effects of zero-point energies, vibrational entropies, and dynamical contributions to the H_2 equation of state.

Figure 3 shows the DFT calculated $T=0$ K static energetics of decomposition for the $Ca(AlH_4)_2$ system. The energetics are shown for four distinct hydrogen contents, corresponding to stoichiometries $Ca(AlH_4)_2$, $CaAlH_5$, CaH_2, and $CaAl_2$. At each stoichiometry, we are plotting the sum of the energies of the coexisting phases versus the number of desorbed H_2 molecules. A necessary condition for the stability of all four phases is that their energetics must lie on a "convex hull," a construction familiar from studies of alloys and compounds, but perhaps less so in the hydrogen storage field. Each of the structures' energies must lie below the straight line connecting the two adjacent energies, thus forming a "hull" which is convex downward. Any energy which does

not fall below the linear combination of adjacent phases would indicate an instability towards phase separation into these two phases. We note from Fig. 3 that with our lowest-energy predicted phases, all four stoichiometries lie on a convex hull, consistent with the observed decomposition sequence. We note, however, that having the energetics lie on a convex hull is merely a necessary, but not sufficient condition for thermodynamic stability: $Ca(AlH_4)_2$ decomposes exothermically at ambient pressure and is thus unstable with respect to decomposition into $CaAlH_5+Al+3/2H_2$. $Ca(AlH_4)_2$ can only be stabilized thermodynamically by application of high H_2 pressure.

When the energies are plotted in the manner of Fig. 3, the energetics of decomposition associated with reactions such as Eq. (2) are given a simple graphical interpretation: these decomposition energies (per mol H_2) are simply the slopes of the lines connecting the points on the convex hull. This graphical interpretation also dictates that the energetics of decomposition must become monotonically more endothermic as the decomposition proceeds (since the slopes must get higher as one moves to the right in Fig. 3 in order to keep the phases on the convex hull). Our calculated energies of decomposition show this monotonic rise: −4.8, +29.8, and +70.3 kJ/mol H_2 for the three reactions in Eq. (2). This simple graphical interpretation of $T=0$ K stability and its implications for the monotonic increase in enthalpies during decomposition is not specific to the Ca-Al-H system, but should hold generally for hydrogen storage decomposition reactions. For example, for the decomposition of sodium alanate via Eq. (1), the first step enthalpy is +37 kJ/mol H_2 and the second is more endothermic at +47 kJ/mol H_2.[21] Subsequent decomposition of NaH occurs at the highest endothermic value of +113 kJ/mol H_2. Many other examples exist of hydrogen storage reactions that illustrate this concept.

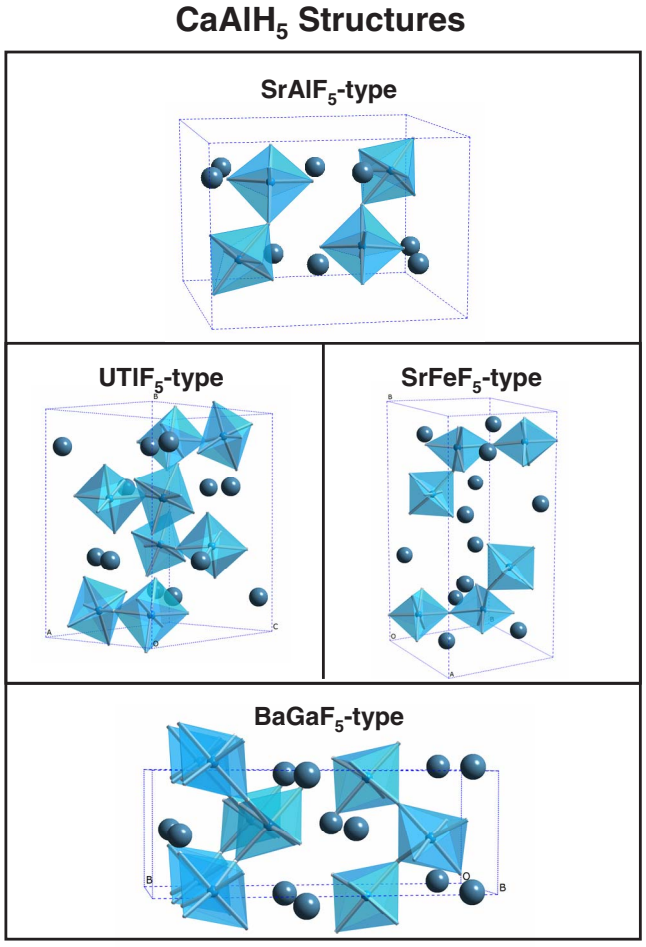

FIG. 2. (Color online) DFT-predicted low-energy structures found for the $CaAlH_5$ stoichiometry. Large spheres are Ca atoms, and Al are centered in polyhedra. For visual clarity, H atoms are not shown, but are at vertices of polyhedra.

E. High-temperature thermodynamic properties

For the low-energy $T=0$ K phases, we have performed DFT frozen-phonon calculations to ascertain the zero-point and vibrational entropy contributions to the thermodynamics of decomposition. The phonon spectra are discussed in the next section. Table V gives the calculated static energetics, vibrational, and dynamic contributions to the decomposition energies in the calcium alanate system. As stated above, we computed the vibrational energies and entropies using US pseudopotential calculations, so we first needed to verify that the US and PAW potential calculations give similar energetics for the static $T=0$ calculations. Table V shows that the US and PAW potentials give extremely similar energetics. The zero-point energies (ZPE) in Table V *decrease* the static enthalpies by about 7–14 kJ/mol H_2. The T-dependent contribution to the enthalpy (the sum of the dynamic $7/2kT$ contribution to the H_2 equation of state and the vibrational enthalpy) *increases* the enthalpies by 4–8 kJ/mol H_2, returning them nearly to the static $T=0$ K values. Another contribution to thermodynamics of these decomposition reactions that is often neglected in DFT studies of hydrogen storage reactions is the vibrational entropies. Our calculated values indicate that these vibrational entropies can contribute up to $4k_B$ [or 33 J/(mol K)] per H_2 molecule, approximately 25% of the entropy of the gas phase in the standard state. Thus, the vibrational entropy can be an important contribution for a quantitatively accurate calculation of the thermodynamics of hydrogen storage reactions.

The validity and accuracy of our approach can be illustrated by comparison with the recent experimental measurements of Mamatha *et al.*[8] on the decomposition of calcium alanate. The comparison between DFT and experimental enthalpies is shown in Table VI, along with the theoretical gravimetric and volumetric densities for the reactions considered. Mamatha *et al.*[8] find that the decomposition of $Ca(AlH_4)_2$ into $CaAlH_5$ occurs at about 127 °C and is weakly exothermic, with an enthalpy of −7 kJ/mol H_2. Our DFT calculated result −9.0 kJ/mol H_2 at $T=127$ °C) is in excellent agreement. Subsequent decomposition of $CaAlH_5$ into CaH_2 at ~250 °C is measured to be endothermic with an enthalpy of +32 kJ/mol H_2, and the DFT result is also endothermic and of similar magnitude (+26.2 kJ/mol H_2 at $T=250$ °C). This reaction of $CaAlH_5$ decomposing into CaH_2 has a gravimetric density of 4.2 wt % and a volumetric

TABLE IV. Structural parameters for the $CaAlH_5$, CaH_2, and $CaAl_2$ compounds in their observed structures. The DFT (VASP) and experimental parameters are given for comparison.

Structure	Prototype	Space group	Structural parameters (DFT)	Structural parameters (Expt.)[a]
$CaAlH_5$	α'-$SrAlF_5$	$P2_1/n$	a=8.334	a=8.3797
			b=6.927	b=6.9293
			c=9.709	c=9.8138
			β=93.88	β=93.78
CaH_2	Co_2Si	$Pnma$	a=5.884 Å	a=5.925 Å
			b=3.568 Å	b=3.581 Å
			c=6.756 Å	c=6.776 Å
			x_{Ca}=0.240	x_{Ca}=0.2378
			z_{Ca}=0.109	z_{Ca}=0.1071
			x_H=0.355	x_H=0.3573
			z_H=0.427	z_H=0.4269
$CaAl_2$	Cu_2Mg	$Fd\bar{3}m$	a=8.016 Å	a=8.035 Å

[a]Reference 10 for $CaAlH_5$, Ref. 30 for CaH_2 and $CaAl_2$.

density of 71.2 g H_2/L, and is near the targeted window of enthalpies suitable for near-ambient hydrogen storage. Hence, though the gravimetric density of this reaction is relatively low, we suggest that the thermodynamics and kinetics of $CaAlH_5$ decomposition should be more fully investigated.

Further decomposition involves the CaH_2 phase. CaH_2 is generally regarded to be much too strongly bound to form a suitable hydrogen storage material. But Al provides an interesting destabilization effect on CaH_2: Our DFT calculations of the decomposition of $CaH_2 \rightarrow Ca+H_2$ give a very large endothermic enthalpy of +172 kJ/mol H_2. However, when Al is added to CaH_2, the decomposition proceeds not via Ca metal, but rather via the strongly bound compound $CaAl_2$. The products of decomposition are thus strongly stabilized by the addition of Al, and hence the decomposition of CaH_2 is strongly destabilized. From Table V, we see that the size of the destabilization is very large, as the enthalpy of CaH_2 +2Al decomposition drops to +72 kJ/mol H_2, a destabilization of +100 kJ/mol H_2, compared to CaH_2 alone. The magnitude of this effect is precisely given by the formation energy of $CaAl_2$, which is known experimentally and theoretically[22] to be $\sim$−100 kJ/mol formula unit. We note that this destabilization effect via stabilization of the products is analogous to the idea initially proposed by Reilly and Wiswall[23] and more recently demonstrated by Vajo *et al.*[24] These types of destabilized reactions have also been studied using DFT by Alapati *et al.*[25] who also calculated the static energetics of the destabilization of CaH_2 by Al and many reactions involving $Ca(AlH_4)_2$. However, we also note that these authors do not consider the presence of the $CaAlH_5$ phase in their decomposition reactions. Vajo *et al.* experimentally demonstrated the destabilization of MgH_2 by addition of Si, forming a Mg_2Si compound. In this case, the energetics go from +75.3 kJ/mol H_2 for pure MgH_2 to

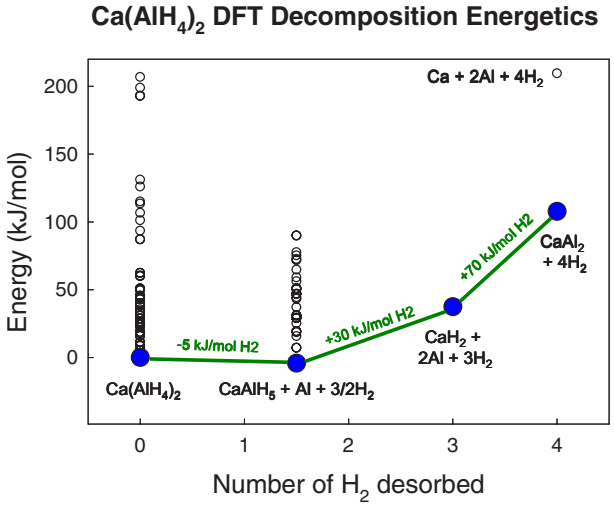

FIG. 3. (Color online) DFT-predicted energetics of decomposition in the $Ca(AlH_4)_2$ system. Each of the energies in our structural database for $Ca(AlH_4)_2$ and $CaAlH_5$ is shown as small open circles (some high-energy structures are excluded from this figure). The lowest-energy structure in each case is a large solid circle. The energetics of decomposition are given by the slopes of the lines connecting the various phases. Note that in this figure, only static, T=0 K energetics are included. The effects of zero-point energies, vibrational entropies, and dynamical contributions to the H_2 equation of state are included in Table V and discussed in the text.

TABLE V. DFT-predicted energetics of decomposition in the $Ca(AlH_4)_2$ system. The static, T=0 K energetics are given for both PAW and US potentials. The effects of zero-point energies (ZPE) are indicated, as are the full dynamic calculations (T=300 K) which include additional contributions from the vibrational energies and the enthalpy of H_2 gas. In the last column, the contribution purely due to vibrational entropy (ΔS_{vib}) is given.

Reaction	Reaction enthalpy ΔH (kJ/mol H_2)				ΔS_{vib} (k_B/H_2)
	Static, PAW	Static, US	With ZPE	T=300 K	T=300 K
$Ca(AlH_4)_2 \rightarrow CaH_2+2Al+3H_2$	+12.5	+12.2	+1.5	+7.2	−2.4
$Ca(AlH_4)_2 \rightarrow CaAlH_5+Al+3/2\ H_2$	−4.8	−5.3	−12.9	−9.0	−4.1
$CaAlH_5 \rightarrow CaH_2+Al+3/2\ H_2$	+29.8	+29.6	+15.9	+23.4	−0.8
$CaH_2+2\ Al \rightarrow CaAl_2+H_2$	+70.3	+70.2	+63.4	+71.7	−0.2
$CaH_2 \rightarrow Ca+H_2$	+172.1	+168.8	+161.1	+170.3	+1.4

TABLE VI. Summary of hydrogen densities and energetics of decomposition in the $Ca(AlH_4)_2$ system. Note that both gravimetric and volumetric densities quoted here are theoretical, single-crystal values. Volumetric densities were calculated from the density of the parent compound (left-hand side of the reaction) multiplied by the fraction of H_2 released from the parent compound. In all cases, the volume of the solid-state products (right-hand side of the reaction) is smaller than the volume of the parent compound.

Reaction	Theoretical gravimetric density (wt %)	Theoretical volumetric density (g H_2/L)	ΔH(T) (kJ/mol H_2) DFT	ΔH (kJ/mol H_2) Expt.[a]
$Ca(AlH_4)_2 \rightarrow CaH_2 + 2\ Al + 3\ H_2$	5.9	69.4	+7.2 (T=300 K)	
$Ca(AlH_4)_2 \rightarrow CaAlH_5 + Al + 3/2\ H_2$	2.9	34.7	−9.0 (T=127 °C)	−7 ($T\sim$127 °C)
$CaAlH_5 \rightarrow CaH_2 + Al + 3/2\ H_2$	4.2	71.2	+26.2 (T=250 °C)	+32 ($T\sim$250 °C)

[a]Reference 8.

+36.4 kJ/mol H_2 to the MgH_2/Si mixture, a destabilization of 39 kJ.[24] The reason that this effect is significantly smaller than the CaH_2/Al example above is twofold: (a) the formation energy of Mg_2Si (Experimental, −63±8 kJ/mol formula unit; DFT, −54 kJ/mol formula unit[26]) is smaller in magnitude than Al_2Ca (∼−100 kJ/mol formula unit), and (b) because the stabilizing compound formed is Mg rich, the ratio of MgH_2:Si is also 2:1, so the destabilizing contribution (per H_2) is only one-half the formation energy of Mg_2Si.

F. Vibrational properties of calcium alanates

Calcium alanate provides an interesting case where markedly different Al-H coordination types are competitive in energy, motivating the need to understand the trends in phonons and their effect on the thermodynamic stability as a function of structure. We reiterate that two tetrahedrally coordinated structures (CaB_2F_8 and β-$ThMo_2O_8$) are predicted to be the lowest in energy of all the considered AB_2X_8 structures. Within 10 kJ/mol of the lowest CaB_2F_8 structure, we find two other structures with unexpected Al-H coordinations. The $AgAu_2F_8$ structure has chains of edge-sharing AlH_6 octahedra, while the $PbRe_2O_8$ structure has chains of corner-sharing AlH_5 pentahedra extending along the hexagonal [0001] direction. We have calculated phonons for $Ca(AlH_4)_2$ in all four of these structures. The calculated phonon DOS curves are shown in Fig. 4. We have used supercells of $88(1\times1\times1)$, $99(1\times1\times1)$, $132(3\times1\times2)$, and $99(1\times1\times3)$ atoms for CaB_2F_8, β-$ThMo_2O_8$, $AgAu_2F_8$, and $PbRe_2O_8$, respectively. The phonon DOS curves were ob-

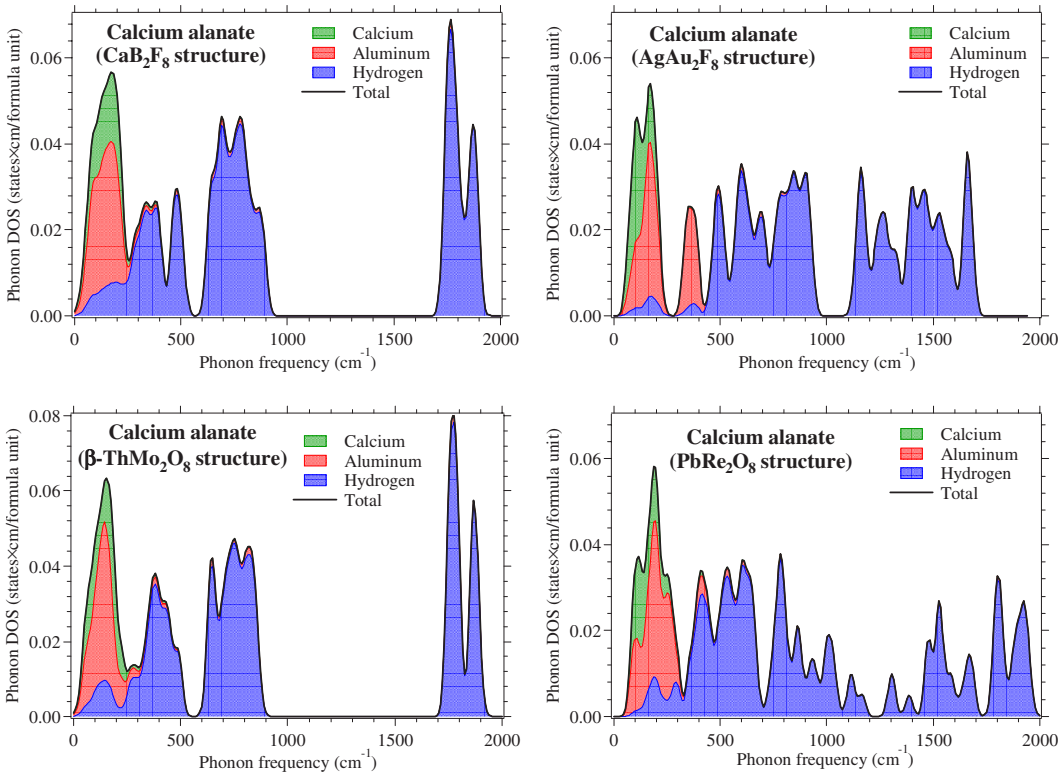

FIG. 4. (Color online) Calculated phonon DOS in the four lowest-energy structures of $CaAl_2H_8$.

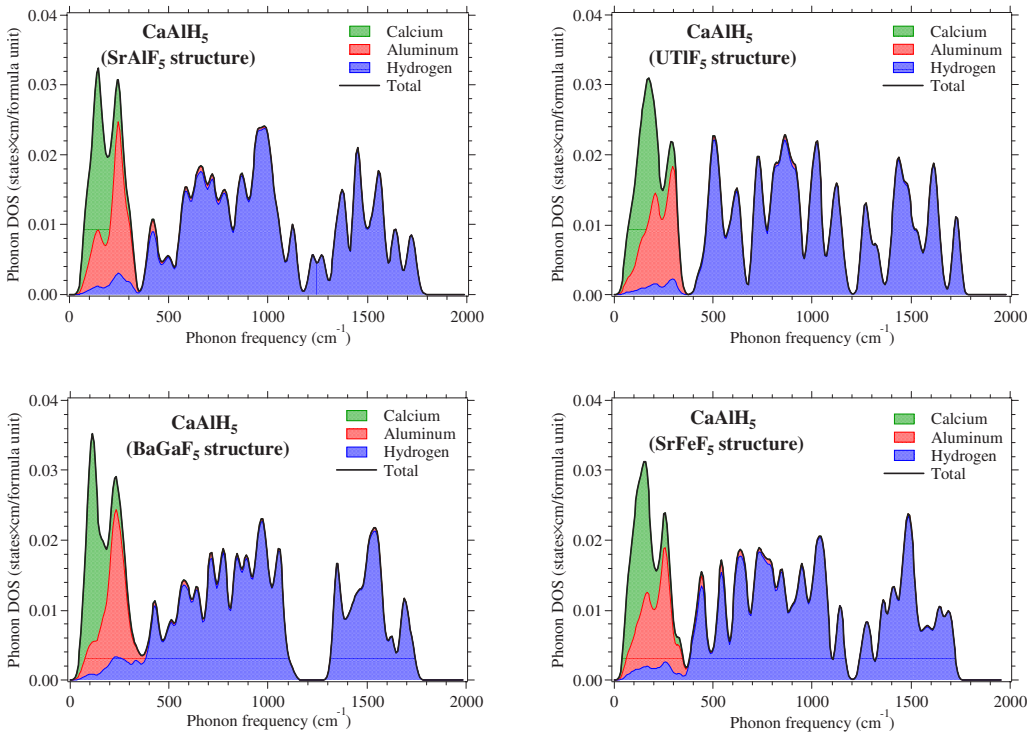

FIG. 5. (Color online) Calculated phonon densities of states for $CaAlH_5$ in the four lowest-energy crystal structures found in this study.

tained by representing the directly calculated frequencies by Gaussians of width 25 cm^{-1}. This broadening should be kept in mind when comparing the exact values of the frequencies mentioned in the text with the DOS curves shown in the figures.

The lattice dynamics of $Ca(AlH_4)_2$ in the lowest-energy CaB_2F_8 structure (shown in the top-left panel of Fig. 4) resemble the well-studied case of $NaAlH_4$,[27–29] although there are some interesting quantitative variations due to differences in ionic masses and stoichiometry. As in $NaAlH_4$, low-energy modes with frequencies below 220 cm^{-1} involve relative motions of Ca ions and AlH_4 tetrahedra. Following the classification scheme adopted in Ref. 27, we will refer to these as translational modes. There are nine such modes per formula unit. At higher frequencies, between 230 and 510 cm^{-1}, we find librational modes characterized by rigid rotations of AlH_4 tetrahedra (six modes per formula unit). Unlike the case of $NaAlH_4$, the librational modes are not separated by a frequency gap from the translational modes. Overall, the frequencies of the librational modes in $Ca(AlH_4)_2$ are substantially lower than those in $NaAlH_4$, indicating that the changed stoichiometry allows for easier rotation of the AlH_4 tetrahedra. In the region from 620 to 900 cm^{-1}, we find phonons that involve bending of H-Al-H bond angles within the AlH_4 tetrahedra. The frequencies of these modes are very similar to those in $NaAlH_4$, but in $Ca(AlH_4)_2$ they are separated from the librational modes by a gap of more than 100 cm^{-1}, Finally, at the highest frequencies between 1740 and 1900 cm^{-1} we find phonons that stretch elastically stiff Al-H bonds (8 modes/f.u.). Since the Al-H bond lengths in $Ca(AlH_4)_2$ are slightly shorter than those in $NaAlH_4$, the Al-H stretch modes lie approximately 100 cm^{-1} higher in energy than those found in $NaAlH_4$. The phonon DOS of the other energetically competitive tetrahedral structure, β-$ThMo_2O_8$, shown in the bottom-left panel of Fig. 4, is very similar to the phonon DOS of the CaB_2F_8 structure. The calculated zero-point vibrational energies and harmonic vibrational entropies of the CaB_2F_8 and β-$ThMo_2O_8$ structures are equal to within the numerical accuracy of our calculations. Since the calculated static energy difference between these structures is quite substantial ($\sim$5 kJ/mol formula unit), our results do not support the possibility that harmonic vibrations could stabilize a high-temperature β-$ThMo_2O_8$ structure below typical decomposition temperatures of calcium alanate ($\sim$127 °C).

Our calculated phonon DOS of the CaB_2F_8 structure is in good agreement with the experimental infrared (IR) spectra of Mamatha *et al.*[8] In particular, their results show the presence of a broad absorption peak centered at 1800 cm^{-1}, which we identify with the Al-H stretch modes. Another strongly absorbing region is observed between 600 and 900 cm^{-1}, which corresponds very well to our calculated frequencies of the H-Al-H bond-bending modes. As we shall see below, the phonons of the nontetrahedral $AgAu_2F_8$ and $PbRe_2O_8$ structures are inconsistent with the IR results of Mamatha *et al.*,[8] which strongly suggests the presence of tetrahedral coordination in $Ca(AlH_4)_2$.

The phonon DOS of $Ca(AlH_4)_2$ in the $AgAu_2F_8$ structure, shown in the top-right panel of Fig. 4, is dramatically different from the phonon DOS of the tetrahedrally coordinated CaB_2F_8 and β-$ThMo_2O_8$ structures. First, because the interlinked edge-sharing AlH_6 octahedra cannot move independently, there are fewer purely translational modes than in the CaB_2F_8 structure. Instead, there is a group of modes at

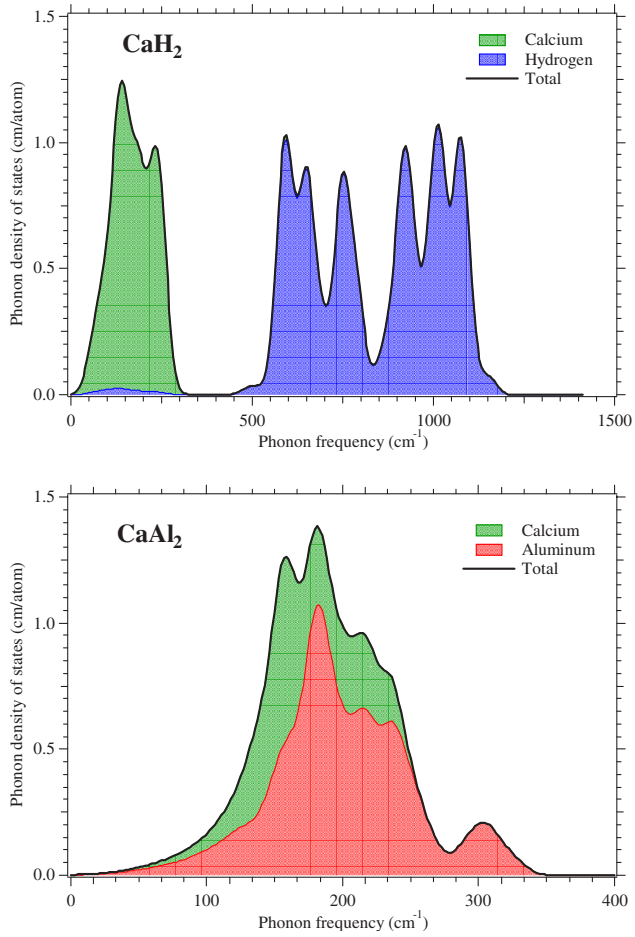

FIG. 6. (Color online) Calculated phonon DOS of CaH_2 and $CaAl_2$.

360 cm^{-1} corresponding to vibrations of Al ions inside the AlH_6 octahedra. Second, there are also fewer purely librational modes; instead, the frequency region between 500 and 900 cm^{-1} contains mixed modes that involve librations and H-Al-H bond-bending motions. Third, in marked difference to the CaB_2F_8 case, the high-frequency region above 1000 cm^{-1} includes 12 (and not 8) Al-H bond-stretching modes per formula unit. The additional four high-frequency modes are located on the shared H ions. Each of the four shared H ions has two nearly perpendicular Al-H bonds (the Al-H-Al bond angles are 96° and 100°), which result in additional constraints on their motion—all movements within the Al-H-Al plane result in an energetically costly Al-H stretching motion. Only the motion perpendicular to this plane can occur without Al-H stretch. In contrast, the nonshared H ions can move in two mutually perpendicular directions without stretching Al-H bonds. Due to the presence of additional high-frequency Al-H stretch modes, the zero-point energy of the edge-shared octahedral $AgAu_2F_8$ structure is 10 kJ/mol higher than that of the tetrahedral $CaBa_2F_8$ structure. This finding is somewhat surprising, since a simpleminded examination of bond lengths shows that $AgAu_2F_8$ has longer Al-H bonds than the CaB_2F_8 structure, and therefore one could expect lower average frequencies and lower zero-point energies.

The $PbRe_2O_8$ structure is characterized by chains of corner-sharing AlH_5 pentahedra, which extend along the hexagonal [0001] direction. We found a slightly unstable optical mode with an imaginary frequency (50*i* cm^{-1}). Frozen-phonon calculations along the eigenvector of the unstable mode showed that the energy curve as a function of the phonon amplitude has an asymmetric double-well shape. Full structural optimizations were performed starting from the configurations corresponding to both minima of the energy curve. The resulting monoclinic structures were less than 0.2 kJ/mol lower in energy, and the ionic positions differed by less than 0.1 Å. Since the relaxed low-energy structures differ so little from the starting hexagonal $PbRe_2O_8$ structure, we expect that the high-frequency phonon spectra in both cases will be very similar (at any rate, performing phonon calculations on a structure with 99 atoms in the unit cell and no symmetry would be too expensive). The vibrational spectrum of the hexagonal $PbRe_2O_8$ structure is shown in the bottom-right panel of Fig. 4 (the unstable optical modes are not included). Similar to the previous structures, it shows a band of low-frequency vibrations corresponding to the translational motion of the Ca and Al ions. These are followed by rotational modes of AlH_5 pentahedra and mixed modes involving bending of H-Al-H bonds. The high-frequency region between 1300 and 1960 cm^{-1} involves stretching of Al-H bonds. The Al-H-Al bond angles around the shared H ions are nearly straight (167° and 170°). Thus, each shared hydrogen is free to move within the basal plane without deforming the Al-H bonds longitudinally, and just like for the tetrahedral CaB_2F_8 case, the high-frequency Al-H stretching region contains eight modes per formula unit. Movement of the shared H along the [0001] direction leads to simultaneous stretching of two Al-H bonds, suggesting that the corresponding frequencies should be roughly a factor of $\sqrt{2}$ higher. However, these bonds are fairly long (1.714, 1.763, 1.773, and 1.816 Å) in comparison with the Al-H bonds for nonshared H (1.673 and 1.695 Å), and the increase in frequencies is offset by the reduced stiffness of each Al-H bond. As a result, the shared H ions exhibit roughly the same frequencies as the nonshared H ions. The total zero-point energy of Ca alanate in the $PbRe_2O_8$ structure is only a few kJ/mol above that of the tetrahedral CaB_2F_8 structure.

All four low-energy structures of $CaAlH_5$ have similar topologies, all characterized by corner-sharing AlH_6 octahedra. As a consequence, there are broad similarities in their calculated phonon DOS curves; see Fig. 5. All four structures have six modes per formula unit in the low-frequency region from 65 to 320 cm^{-1}, corresponding to vibrational motions of Ca and Al ions. It is interesting to note the difference in these modes in comparison with the translational modes in the tetrahedrally coordinated CaB_2F_8 structure of $Ca(AlH_4)_2$ in Fig. 4. In particular, the former extend to higher frequencies (320 instead of 220 cm^{-1}) and show less participation of H ions. We attribute this difference to the structural features of $CaAlH_5$: since it contains buckled chains of corner-shared AlH_6 octahedra, low-energy modes cannot involve rigid movements of these octahedra alone, but must also involve some degree of deformation in the Al-H bond lengths and bond angles. The system achieves this by leaving H ions mostly static and moving only Ca and Al ions. In contrast, in

the CaB_2F_8 structure the tetrahedral AlH_4 units are independent and can move as a whole. At higher energies in the frequency region 430–660 cm^{-1} we have modes describing coupled rotations of AlH_6 octahedra. These modes are intermixed with the higher-frequency (715–1150 cm^{-1}) phonon modes that involve H vibrations deforming the H-Al-H bond angles and a clear separation between the two types is difficult. In the highest-frequency region between 1200 and 1700 cm^{-1} we find phonon modes involving changes in Al-H bond lengths. For each formula unit, there are five such modes. The $BaGaF_5$ structure shows the clearest separation between these Al-H stretching and H-Al-H bending modes, with an energy gap of slightly more than 200 cm^{-1}. In the $BaGaF_5$ structure they also start at a higher frequency than in the other two competing structures: 1340 vs 1260 cm^{-1}. The calculated vibrational energies and entropies of all four structures in Fig. 5 are very similar, differing by less than a few kJ/mol, which we consider to be within the numerical errors of our calculations due to finite supercell sizes.

The calculated phonon DOS of CaH_2 and $CaAl_2$ are shown in Fig. 6. In CaH_2, we find a band of low-frequency Ca vibrations up to 250 cm^{-1} and high-frequency optical H modes between 500 and 1150 cm^{-1}. The $CaAl_2$ structure exhibits strong mixing of Ca and Al character throughout the frequency spectrum.

IV. CONCLUSIONS

We have used first-principles DFT calculations to study the crystal structures, thermodynamics, and vibrational properties of calcium alanate and its decomposition products: $Ca(AlH_4)_2$, $CaAlH_5$, CaH_2, and $CaAl_2$. For $Ca(AlH_4)_2$ and $CaAlH_5$, we have performed an extensive number of ~200 DFT calculations of chemically similar crystal structure types taken from the ICSD in an effort to predict the structures of these phases. For $Ca(AlH_4)_2$, we find that the CaB_2F_8-type structure is lowest in energy, but that β-$ThMo_2O_8$-type, $AgAu_2F_8$-type, and $PbRe_2O_8$-type structures are energetically competitive. In the case of $CaAlH_5$, the α'-$SrAlF_5$-type structure has the lowest energy, but again, there are other structural types very close in energy: $UTlF_5$-type, $SrFeF_5$-type, and $BaGaF_5$-type structures. For these low-energy structures, we have performed DFT frozen-phonon calculations to ascertain the vibrational properties and thermodynamic functions. The structure types show a variety of local coordination types, and our phonon calculations can be largely rationalized by considering the translational and librational modes of the ionic units, as well as the bond-bending and bond-stretching modes of the AlH_x anions ($x=4,5,6$).

By combining our energetic and phonon calculations, we give DFT predictions of the thermodynamics of decomposition for Ca alanate. In agreement with recent experiments, our calculations show that the decomposition of $Ca(AlH_4)_2$ is divided into a weakly exothermic step [$Ca(AlH_4)_2 \rightarrow CaAlH_5 + Al + 3/2H_2$], a weakly endothermic step [$CaAlH_5 \rightarrow CaH_2 + Al + 3/2H_2$], and a strong endothermic step [$CaH_2 + 2Al \rightarrow CaAl_2 + H_2$]. Including static $T=0$ K energies, zero-point energies, and the dynamic contributions of H_2 gas gives predicted enthalpies in close agreement with experimental values. The second, weakly endothermic step [$CaAlH_5/CaH_2$] has thermodynamics near the targeted range that might make a suitable on-board hydrogen storage reaction for hydrogen-fueled vehicles, and we suggest that further investigation of this reaction would be of interest. For the final stage of decomposition [$CaH_2 + 2Al \rightarrow CaAl_2 + H_2$], we note that the addition of Al provides a huge destabilizing effect on CaH_2, due to the formation of the strongly bound $CaAl_2$ phase.

ACKNOWLEDGMENTS

V.O. thanks the U.S. Department of Energy for financial support under Grants No. DE-FG02-05ER46253 and No. DE-FC36-04GO14013.

[1] See http://www.eere.energy.gov/hydrogenandfuelcells/storage/pdfs/targets_onboard_hydro_storage.pdf
[2] L. Schlapbach and A. Züttel, Nature (London) **414**, 353 (2001); G. Sandrock and R. C. Bowman, Jr., J. Alloys Compd. **356–357**, 794 (2003).
[3] B. Bogdanovic and M. Schwickardi, J. Alloys Compd. **253**, 1 (1997).
[4] T. N. Dymova, D. P. Aleksandrov, V. N. Konoplev, T. A. Silina, and A. S. Sizareva, Russ. J. Coord. Chem. **20**, 263 (1994); N. N. Mal'tseva, and A. I. Golovanova, Russ. J. Appl. Chem. **73**, 747 (2000); O. M. Lovvik, S. M. Opalka, H. W. Brinks, and C. Hauback, Phys. Rev. B **69**, 134117 (2004).
[5] E. Wilberg and R. Bauer, Z. Naturforsch. B **7**, 131 (1952); T. N. Dymova, V. N. Konoplev, A. S. Sizareva, and D. P. Aleksandrov, Russ. J. Coord. Chem. **25**, 312 (1999); M. Fichtner, J. Engel, O. Fuhr, A. Gloss, O. Rubner, and R. Ahlrichs, Inorg. Chem. **42**, 7060 (2003).
[6] W. Schwab and K. Wintersberger, Z. Naturforsch. B **8**, 690 (1953).
[7] N. N. Mal'tseva, A. I. Golovanova, T. N. Dymova, and P. Aleksandrov, Russ. J. Inorg. Chem. **46**, 1793 (2001).
[8] M. Mamatha, B. Bogdanovic, M. Felderhoff, A. Pommerin, W. Schmidt, F. Schuth, and C. Weidenthaler, J. Alloys Compd. **407**, 78 (2006).
[9] O. M. Løvvik, Phys. Rev. B **71**, 144111 (2005).
[10] C. Weidenthaler, T. J. Frankcombe, and M. Felderhoff, Inorg. Chem. **45**, 3849 (2006).
[11] P. Hohenberg and W. Kohn, Phys. Rev. **136**, B864 (1964); W. Kohn and L. J. Sham, Phys. Rev. **140**, A1133 (1965).
[12] G. Kresse and J. Hafner, Phys. Rev. B **47**, 558 (1993); G. Kresse, Ph.D. thesis, Technische Universität Wien, 1993; G. Kresse and J. Furthmüller, Comput. Mater. Sci. **6**, 15 (1996); Phys. Rev. B **54**, 11169 (1996).
[13] D. Vanderbilt, Phys. Rev. B **41**, 7892 (1990); G. Kresse and J.

Hafner, J. Phys.: Condens. Matter **6**, 8245 (1994).
[14] P. E. Blöchl, Phys. Rev. B **50**, 17953 (1994).
[15] J. P. Perdew and Y. Wang, Phys. Rev. B **45**, 13244 (1992).
[16] C. Wolverton, V. Ozolins, and M. Asta, Phys. Rev. B **69**, 144109 (2004).
[17] M. Fichtner, J. Engel, O. Fuhr, A. Gloss, O. Rubner, and R. Ahlrichs, Inorg. Chem. **42**, 7060 (2003).
[18] P. Vajeeston, P. Ravindran, A. Kjekshus, and H. Fjellvåg, J. Alloys Compd. **363**, L7 (2004); O. M. Løvvik and O. Swang, Europhys. Lett. **67**, 607 (2004).
[19] E. M. Larson, P. G. Eller, T. L. Cremers, R. A. Penneman, and C. C. Herrick, Acta Crystallogr., Sect. C: Cryst. Struct. Commun. **45**, 1669 (1989).
[20] A. Klaveness, P. Vajeeston, P. Ravindran, H. Fjellvåg, and A. Kjekshus, Phys. Rev. B **73**, 094122 (2006).
[21] Bogdanovic, R. A. Brand, A. Marjanovic, M. Schwickardi, and J. Tolle, J. Alloys Compd. **302**, 36 (2000).
[22] K. Ozturk, Y. Zhong, L.-Q. Chen, C. Wolverton, J. O. Sofo, and Z.-K. Liu, Metall. Mater. Trans. A **36**, 5 (2005).
[23] J. J. Reilly and R. H. Wiswall Inorg. Chem. **7**, 2254 (1968); **6**, 2220 (1967).
[24] J. Vajo, F. Mertens, C. Ahn, R. C. Bowman Jr., and B. Fultz, J. Phys. Chem. B **108**, 13977 (2004); J. Vajo, S. Skeith, and F. Mertens. *ibid.* **109**, 3719 (2005).
[25] S. V. Alapati, J. K. Johnson, and D. S. Scholl, J. Phys. Chem. B **110**, 8769 (2006).
[26] H. Feufel, T. Godecke, H. L. Lukas, and F. Sommer, J. Alloys Compd. **247**, 31 (1997); C. Ravi and C. Wolverton, Acta Mater. **52**, 4213 (2004).
[27] E. H. Majzoub, K. F. McCarty, and V. Ozolins, Phys. Rev. B **71**, 024118 (2005).
[28] X. Ke and I. Tanaka, Phys. Rev. B **71**, 024117 (2005).
[29] A. Peles and M. Y. Chou, Phys. Rev. B **73**, 184302 (2006).
[30] P. Villars and L. D. Calvert, *Pearson's Handbook of Crystallographic Data* (ASM International, Materials Park, OH, 1991).